25 °C, it is unlikely to be sufficiently different at 85 °C and 200 MPa to account for this disagreement.

Mechanism B. $Co^{III}(EDTA)^-$ aquates to form $Co(EDTA)OH_2^-$ in an initial step with a volume change ΔV_{aq} of about -10.5 cm^3 mol^{-1} (estimated as explained above); adiabatic electron transfer then occurs between $Co^{III}(EDTA)OH_2^-$ and $Co^{II}(HEDTA)OH_2^-$. Ring opening and aquation in $Co^{III}(EDTA)^-$, however, require prior protonation if the initial step is to be fast enough under the conditions of the electron-transfer experiments, and the rate equation for reaction 1 shows that this does not occur. In any event, the acceleration of reaction 1 predicted on this basis is far too strong (curve B, Figure 1; calculated average $\Delta V_{ex}^{\ddagger} \simeq -16$ cm^3 mol^{-1}).

Mechanism C. $Co^{III}(HEDTA)OH_2^0$ forms as in reaction 2 (which is some 700 times as fast[10e] as the exchange rate at 85 °C, pH 2.0, and the relevant $[Co^{II}]$;[12] measured volume change at 25 °C = -3.2 cm^3 mol^{-1}) and undergoes adiabatic electron exchange with the predominant Co^{II} species, $Co^{II}(HEDTA)OH_2^-$. This nicely symmetrical model, however, would require first-order dependence of the measured electron-transfer rate on $[H^+]$ at pH 2.0 and below, whereas the pH profile shows a plateau in rate in this region. Furthermore, this model predicts an excessive pressure acceleration (curve C in Figure 1; average $\Delta V_{ex}^{\ddagger} \simeq -9.0$ cm^3 mol^{-1} over the pressure range).

Mechanism D. The reaction proceeds as in mechanism A, which is the most likely pathway, but is *nonadiabatic*. In the simplest treatment,[16] this additional constraint requires only the introduction of a distance-scaling parameter α for calculation of the pressure effect on the reaction rate. In practice, α is not easily predictable from theory with the required precision, so it may be introduced as an adjustable parameter to fit the experimental data to within the error bars. This is done in curve D of Figure 1, for which $\alpha = 13 \pm 1$ nm^{-1}—a value that is midrange for reactions of this type[31] and is similar to that (16–19 nm^{-1}) estimated in the same way for the $Co(en)_3^{3+/2+}$ exchange.[30]

Two further possibilities may be considered: an inner-sphere electron-transfer mechanism involving one of the carboxylate groups of the two EDTA ligands as a ligand bridge, and H atom transfer rather than electron transfer in mechanism A (cf. Figure 2). The first may be discounted because there was no evidence of bridging-ligand trapping by the newly formed Co^{III} center to give a binuclear complex; the Co^{III} and Co^{II} fractions separated cleanly after exchange. The second remains a real possibility, but at present it is not possible to say how it would be manifested in terms of pressure effects, and accordingly it has not been considered further.

Thus, if it is accepted that the exchange process at pH 2 is of the outer-sphere type, then the kinetic effect of pressure is consistent with nonadiabatic electron transfer between the predominant Co species in solution, $Co^{III}(EDTA)^-$ and $Co^{II}(HEDTA)OH_2^-$, following rapid deaquation of the latter (mechanism D). This places reaction 1 in the same mechanistic category as the $Co(en)_3^{3+/2+}$ exchange in water, for which the strong acceleration by pressure has been ascribed to nonadiabaticity of electron transfer.[30,32] Significantly, both the $Co(en)_3^{3+/2+}$ and the $Co(EDTA)^-/Co(HEDTA)OH_2^-$ exchanges are much slower than the analogous $Co(sep)^{3+/2+}$ and $Co([9]aneS_3)_2^{3+/2+}$ reactions, the rates and volumes of activation of which are consistent with full adiabaticity.[32,33]

On a final note of caution, we remark that all of these models predict that plots of ln (k/k_0) vs P for outer-sphere electron transfer should be distinctly curved,[16] yet the experimental data seem to be better represented by a linear regression. Similar seemingly excessive curvatures of theoretical ln (k/k_0) vs P plots have been noted in several cases and may reflect a basic inadequacy of the theory.[16]

Acknowledgment. We thank the Australian Research Grants Committee for support. W.H.J. acknowledges financial assistance given by a Commonwealth Postgraduate award. T.W.S. thanks the Norman Thomas Wilsmore Research Fund for the award of a fellowship and the Universities of Melbourne and Adelaide for their generous hospitality.

Registry No. $Co^{III}(EDTA)^-$, 15136-66-0; $Co^{II}(HEDTA)OH_2^-$, 14024-68-1.

(30) Jolley, W. H.; Stranks, D. R.; Swaddle, T. W. *Inorg. Chem.* **1990**, *29*, 385.
(31) Sutin, N. *Prog. Inorg. Chem.* **1983**, *30*, 441.
(32) Doine, H.; Swaddle, T. W. *Inorg. Chem.* **1991**, *30*, 1858.
(33) Hendry and Lüdi[34] point out that the Co–N bond distances change by 21 pm in the $Co(en)_3^{3+/2+}$ exchange and by 19 pm in the $Co(sep)^{3+/2+}$ case; thus, the fact that the former is some 10^5-fold slower than the latter is attributable only in part to differences in the inner-sphere reorganization energies. Substantial nonadiabaticity in the electron-transfer step would therefore seem likely in the $Co(en)_3^{3+/2+}$ case. The $Co(EDTA)^-/Co(HEDTA)OH_2^-$ exchange is 17 times slower than the $Co(en)_3^{3+/2+}$ reaction at 85 °C, pH 2.0, and $I = 0.5$ mol L^{-1}.[30]
(34) Hendry, P.; Lüdi, A. *Adv. Inorg. Chem.* **1990**, *35*, 117.

Contribution from the Department of Chemistry, Virginia Commonwealth University, Box 2006, Richmond, Virginia 23284

Solution IR Spectroscopic Studies of *cis*-Dioxomolybdenum(VI) Complexes

Joseph Topich* and John O. Bachert, III†

Received July 2, 1991

Series of *cis*-dioxo-MoL·DMF complexes have been investigated using FT-IR spectroscopy in DMF solution. The ligands (L) used are obtained from Schiff base condensation of 5-X-salicylaldehyde (X = NO_2, Cl, Br, H, OCH_3) with *o*-aminophenol, *o*-aminobenzenethiol, 2-aminoethanol, 2-aminoethanethiol, 2-amino-5-nitrophenol or 2-amino-4-nitrophenol. Correlations were observed between the antisymmetric Mo=O stretching vibration (ν_{as}(Mo=O)), the Hammett parameter (σ_p) for the X substituent on the salicylaldehyde ligand fragment, and the specific rate constant (k_1) for oxygen atom transfer between $Mo^{VI}O_2$(5-X-SSP) or $Mo^{VI}O_2$(5-X-SSE) and $PEtPh_2$. The observed variation in ν_{as}(Mo=O) as the ligand structure is systematically altered reflects changes in the relative energy of the oxo O π^* antibonding orbital. We propose that this energy change contributes to the activation energy in the oxygen atom transfer reaction with $PEtPh_2$. Our results support the proposed reaction mechanism of donation of the phosphorus lone-pair electrons into the oxo O π^* antibonding orbital.

Introduction

A number of redox enzymes are known to be dependent on molybdenum for physiological activity. Some of these enzymes include nitrate reductase, xanthine oxidase, sulfite oxidase, and aldehyde oxidase. Extended X-ray absorption fine structure (EXAFS) spectroscopy studies[1-4] have implicated sulfur and

† Current address: American Cyanamid Co., P.O. Box 400, Princeton, NJ 08543-0400.

(1) Tullius, T. D.; Kurtz, D. M., Jr.; Conradson, S. D.; Hodgson, K. O. *J. Am. Chem. Soc.* **1979**, *101*, 2776–2779.
(2) Cramer, S. P.; Gray, H. B.; Rajagopalan, K. V. *J. Am. Chem. Soc.* **1979**, *101*, 2772–2774.

0020-1669/92/1331-0511$03.00/0

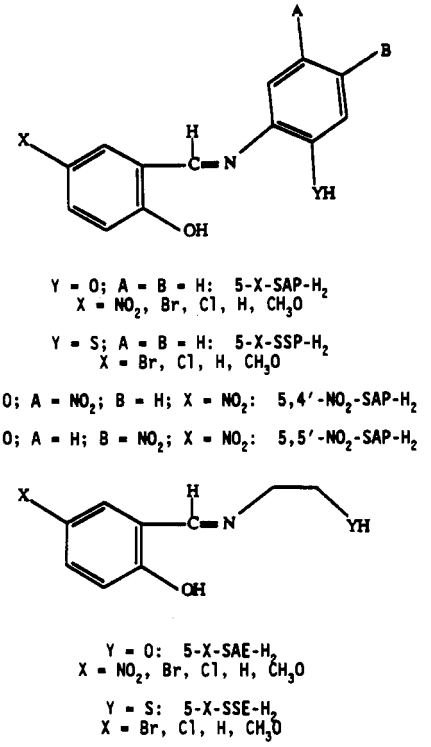

Figure 1. Tridentate Schiff base ligands.

oxygen as ligand donor atoms in the coordination sphere of the molybdenum. In addition, EXAFS data also suggest that the oxidized forms of nitrate reductase and sulfite oxidase[2,3] contain the *cis*-dioxo-Mo^{2+} unit, while the reduced forms of xanthine dehydrogenase and sulfite oxidase contain a single terminal oxo ligand. It is believed that, in the catalytic cycle of these enzymes, the molybdenum undergoes oxidation state changes between the +4, +5, and +6 levels, while remaining mononuclear.

Our laboratory,[5-7] as well as others,[8] have studied the chemical and physical properties of various molybdenum complexes in order to gain a greater insight into the structure/function relationships for these complexes. The chemical information gained in studying the molybdenum coordination complexes may be transferrable to enzyme structure/function questions not readily solvable by studying the enzymes themselves.

It is known at the most fundamental level that the molybdenum enzymes are involved in oxygen atom transfer reactions with substrate.[9] Biochemical studies provide evidence supporting an oxygen atom transfer mechanism in xanthine oxidase.[10] In an effort to better understand oxygen atom transfer reactions mediated by a *cis*-dioxo-Mo^{2+} unit, we have studied reactions between molybdenum coordination complexes containing tridentate Schiff base ligands (see Figure 1) and $PEtPh_2$.

$$Mo^{VI}O_2L + PEtPh_2 \underset{k_{-1}}{\overset{k_1}{\rightleftharpoons}} Mo^{IV}OL + O{=}PEtPh_2 \quad (1)$$

$$Mo^{VI}O_2L + Mo^{IV}OL \underset{k_{-2}}{\overset{k_2}{\rightleftharpoons}} Mo^{V}_2O_3L_2 \quad (2)$$

Reaction 1 is characterized by a second-order rate constant, k_1,[7] the magnitude of which depends on the substitution pattern of the ligand. Additionally, we[5-7] have demonstrated that correlations exist between the cathodic reduction potential (E_{pc}), the Hammett parameter (σ_p), and k_1.

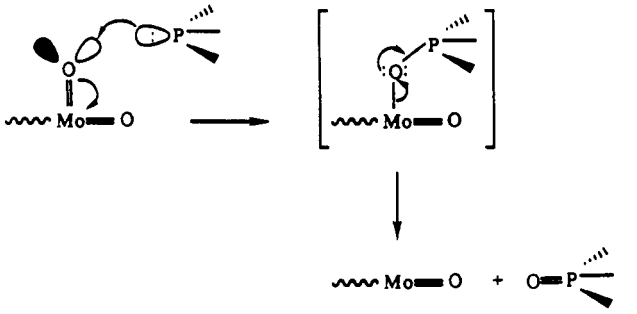

Figure 2. Mechanism for oxygen atom transfer (adapted from ref 13).

Formation of the μ-oxo-Mo(V) dimer (reaction 2) is known to occur in many molybdenum systems.[8] Dimer formation is undesirable from a bioinorganic modeling standpoint since this does not occur in the molybdenum enzymes. Sterically encumbered ligand systems have been designed[9,11] to prevent dimer formation. For the molybdenum complexes studied here, dimer formation is not precluded on steric grounds alone. However, in the event of reaction 2, reaction 1 is the rate-limiting process.[12]

The proposed mechanism for reaction 1 involves the donation of the phosphorus lone-pair electrons into an oxo O π^* antibonding orbital of the *cis*-dioxo-Mo^{2+} unit.[13] This is followed by metal reduction (Mo(VI) → Mo(IV)) and product separation (Figure 2).

Since it is an oxo oxygen that is involved in the oxygen atom transfer reaction with phosphines, then monitoring the Mo=O stretching vibrations as a function of ligand substitution within these complexes may provide additional experimental insight into the validity of this mechanism. At the same time this may help to establish plausible criteria as to why certain molybdenum complexes react with organophosphines and others do not (vide infra). To this end we report the FT-IR spectra of the $Mo^{VI}O_2$(5-X-SAP), $Mo^{VI}O_2$(5-X-SSP), $MO^{VI}O_2$(5-X-SAE), and $Mo^{VI}O_2$(5-X-SSE) complexes obtained in DMF solution and present correlations which have been established between σ_p, k_1, and ν(Mo=O). These results will be discussed with regard to the chemical properties of these complexes, particularly with reference to the mechanism of the oxygen atom transfer reaction.

Experimental Section

Preparation of Ligands and Molybdenum Complexes. $Mo^{VI}O_2$(5-X-SAP), $Mo^{VI}O_2$(5-X-SAE), $Mo^{VI}O_2$(5-X-SSE), and $Mo^{VI}O_2$(5-X-SSP) were synthesized as described by Topich et al.[5,14] $Mo^{VI}O_2(S_2CNEt_2)_2$ was synthesized according to the method of Jowitt and Mitchell.[15]

The ligands 5,5'-NO_2-SAP-H_2 and 5,4'-NO_2-SAP-H_2 were synthesized via Schiff base condensation reactions between 5-nitrosalicylaldehyde and either 2-amino-5-nitrophenol or 2-amino-4-nitrophenol. The corresponding $Mo^{VI}O_2$(5,5'-NO_2-SAP) and $Mo^{VI}O_2$(5,4'-NO_2-SAP) complexes were obtained by refluxing $Mo^{VI}O_2(acac)_2$ and the appropriate ligand in absolute ethanol. The molybdenum complexes were isolated by vacuum filtration and recrystallized from DMSO and water.[14] *N,N*-Dimethylformamide was purchased from American Burdick and Jackson and dried over type 3A molecular sieves. Elemental analyses were performed by Atlantic Microlabs. Anal. Found (calcd) for $Mo^{VI}O_2$(5,5'-NO_2-SAP)·$(CH_3)_2SO$: C, 35.27 (35.51); H, 2.46 (2.58); N, 8.16 (8.28). Anal. Found (calcd) for $Mo^{VI}O_2$(5,4'-NO_2-SAP)·$(CH_3)_2SO$: C, 35.34 (35.51); H, 2.51 (2.58); N, 8.18 (8.28).

Physical Measurements. FT-IR spectra were obtained in DMF solution using a Nicolet-740 FT-IR spectrophotometer. Solution spectra were obtained in a Harrick 9-reflection prism liquid cell employing a ZnSe crystal. Peak maxima were determined by applying the Nicolet "peak-picking" algorithm to the spectra. The peak maxima (in cm^{-1})

(3) Berg, J. M.; Hodgson, K. O.; Cramer, S. P.; Corbin, J. L.; Elsberry, A.; Pariyadath, N.; Stiefel, E. I. *J. Am. Chem. Soc.* **1979**, *101*, 2774–2776.
(4) Cramer, S. P.; Wahl, R.; Rajagopalan, K. V. *J. Am. Chem. Soc.* **1981**, *103*, 7721–7727.
(5) Topich, J.; Lyon, J. T. *Polyhedron* **1984**, *3*, 55–60.
(6) Topich, J.; Lyon, J. T. *Polyhedron* **1984**, *3*, 61–65.
(7) Topich, J.; Lyon, J. T. *Inorg. Chem.* **1984**, *23*, 3202–3206.
(8) Reynolds, M. S.; Berg, J. M.; Holm, R. H. *Inorg. Chem.* **1984**, *23*, 3057–3062.
(9) Holm, R. H.; Berg, J. M. *Acc. Chem. Res.* **1986**, *19*, 363–370.
(10) Hille, R.; Sprecher, H. *J. Biol. Chem.* **1987**, *262*, 10914–10917.
(11) Cook, C. J.; Topich, J. *Inorg. Chim. Acta* **1988**, *144*, 81–87.
(12) Craig, J. A.; Harlan, E. W.; Snyder, B. S.; Whitener, M. A.; Holm, R. H. *Inorg. Chem.* **1989**, *28*, 2082–2091.
(13) Durant, R.; Garner, C. D.; Hyde, M. R.; Mabbs, F. E.; Parsons, J. R.; Richens, D. *J. Less-Common Met.* **1977**, *54*, 459–464.
(14) Topich, J. *Inorg. Chem.* **1981**, *20*, 3704–3707.
(15) Jowitt, R. N.; Mitchell, P. C. H. *J. Chem. Soc. A* **1970**, 1702–1708.

Table I. Kinetic, Electrochemical, and IR Data for the Molybdenum(VI) Complexes

Mo(VI) complex	10^4k_1, M^{-1} s^{-1} at 30 °C	10^4k_1, M^{-1} s^{-1} at 60 °C	E_{pc},[a] V	ν(Mo=O),[b] cm^{-1}
$Mo^{VI}O_2$(5-Br-SSP)	19.6 ± 0.6		−0.91	902.1, 933.0
$Mo^{VI}O_2$(5-Cl-SSP)	18.7 ± 0.2		−0.92	902.1, 933.5
$Mo^{VI}O_2$(5-H-SSP)	10.2 ± 0.9	116.0 ± 6.2	−0.97	900.8, 932.1
$Mo^{VI}O_2$(5-CH_3O-SSP)	8.4 ± 0.4		−0.99	900.7, 931.4
$Mo^{VI}O_2$(5-Br-SSE)		34.8 ± 2.8	−1.08	899.8, 930.3
$Mo^{VI}O_2$(5-Cl-SSE)		34.6 ± 2.7	−1.08	900.0, 930.2
$Mo^{VI}O_2$(5-H-SSE)	2.1 ± 0.2	28.1 ± 1.8	−1.11	899.3, 929.6
$Mo^{VI}O_2$(5-CH_3O-SSE)		21.4 ± 0.6	−1.13	899.1, 929.0
$Mo^{VI}O_2$(5,5′-NO_2-SAP)			−0.80	915.8, 939.0
$Mo^{VI}O_2$(5,4′-NO_2-SAP)			−0.80	916.5, 938.8
$Mo^{VI}O_2$(5-NO_2-SAP)			−0.97	913.9, 937.4
$Mo^{VI}O_2$(5-Br-SAP)			−1.03	912.4, 936.2
$Mo^{VI}O_2$(5-Cl-SAP)			−1.03	912.4, 936.0
$Mo^{VI}O_2$(5-H-SAP)			−1.10	911.2, 934.9
$Mo^{VI}O_2$(5-CH_3O-SAP)			−1.11	911.1, 935.0
$Mo^{VI}O_2$(5-NO_2-SAE)			−1.11	909.5, 925.3
$Mo^{VI}O_2$(5-Br-SAE)			−1.34	908.2, 928.0
$Mo^{VI}O_2$(5-Cl-SAE)			−1.34	907.9, 929.5
$Mo^{VI}O_2$(5-H-SAE)			−1.35	906.4, 927.3
$Mo^{VI}O_2$(5-CH_3O-SAE)			−1.39	906.1, 923.7
$Mo^{VI}O_2(S_2CNEt_2)_2$			−0.78	881.2, 912.3

[a] E_{pc} is referenced to SCE with the Fc/Fc^+ couple observed at +0.54 V. [b] Standard deviation is ≤0.2 cm^{-1}.

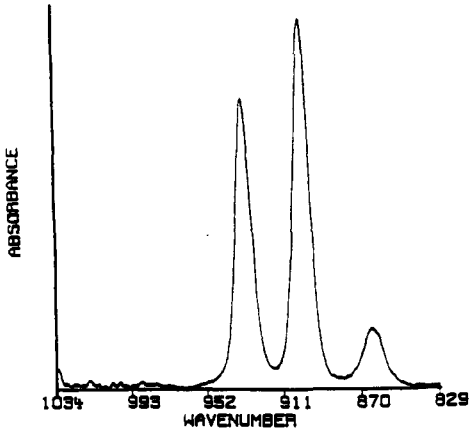

Figure 3. Solution IR absorption spectrum in the Mo=O stretching region for $Mo^{VI}O_2$(5-H-SSP) in DMF after solvent subtraction.

reported in Table I are from the average of between 5 and 15 individual spectra (32 scans/spectrum). The standard deviation is less than or equal to 0.2 cm^{-1}.

Results and Discussion

The coordination geometry for these complexes involves the molybdenum atom bound (in a pseudooctahedral fashion) meridionally to the three donor atoms of the tridentate Schiff base ligand, by the two oxo ligands in a cis configuration, and a solvent molecule (DMF). Figure 3 shows a representative solution FT-IR spectrum of $Mo^{VI}O_2$(5-H-SSP) after solvent (DMF) subtraction. The two strong bands at ~935 and ~900 cm^{-1} are assigned respectively to the symmetric and antisymmetric Mo=O vibrations (vide infra). Table I includes a collection of the Mo=O stretching frequencies assigned to the complexes studied here.

For the *cis*-dioxo-Mo unit (with idealized C_{2v} symmetry), group theoretical considerations indicate the existence of two stretching vibrations, the symmetric (a_1) and the antisymmetric (b_1), that are both IR and Raman active. Raman polarization measurements[16] indicate that the symmetric Mo=O stretching frequencies are higher in energy than the antisymmetric vibrations. Regarding the molybdenum complexes studied here, infrared spectra of the free ligands (solid (KBr) and solution (DMF)) show no vibrations in the ~1000–900-cm^{-1} region, whereas all molybdenum complexes examined display two strong vibrations in this region. X-ray crystallographic results[17] demonstrate the presence of the *cis*-dioxo-Mo core within these complexes. Preliminary resonance Raman data confirm the coincidence in the IR and Raman spectra for the observed vibrations. The signal-to-noise ratio, however, was too low in the Raman spectra for polarization measurements to be obtained.

In some of our previous work,[5-7] we demonstrated correlations between k_1 (reaction 1) and E_{pc} for the series $Mo^{VI}O_2$(5-X-SSP) and $Mo^{VI}O_2$(5-X-SSE). The same electronic effects that cause systematic changes in the E_{pc}'s for these complexes also alters the electrophilic character of the Mo(VI) oxo ligand for its reaction with organophosphines. It was observed that the magnitude of E_{pc} (as measured in DMF) in itself was not sufficient to establish the reactivity of these Mo(VI) complexes toward organophosphines. From Table I it can be seen that for $Mo^{VI}O_2$(5-NO_2-SAE) and the $Mo^{VI}O_2$(5-X-SAP) series, the E_{pc}'s are interleaved with those of the $Mo^{VI}O_2$(5-X-SSE) and $Mo^{VI}O_2$(5-X-SSP) series. The E_{pc} values do not assume distinct potential regions as one might expect based on the reactivity of $Mo^{VI}O_2$(5-X-SSP) and $Mo^{VI}O_2$(5-X-SSE) toward $PEtPH_2$ and the lack of reactivity of $Mo^{VI}O_2$(5-X-SAP) and $Mo^{VI}O_2$(5-X-SAE). It is interesting to observe however, that the frequency of the ν_{as}(Mo=O) stretching vibration does separate into "reactive" and "nonreactive" regions in a manner parallel to the reactivity of these complexes toward $PEtPh_2$. The "non-reactive" molybdenum species fall in a frequency region between ~906 and 916 cm^{-1}, whereas the "reactive" molybdenum species occupy a frequency region between ~899 and 902 cm^{-1}. Additionally, $Mo^{VI}O_2(S_2CNEt_2)_2$, which displays a higher reactivity toward organophosphines as compared to the molybdenum complexes studied here,[7] possesses the lowest ν_{as}(Mo=O) of the complexes collected in Table I.

Correlation of ν_{as}(Mo=O) with Ligand Substituent Parameters. For the correlations that have been established between E_{pc} and σ_p for these molybdenum complexes,[5-7] trends are observed within and between series. These trends are influenced by three principle ligand features: (1) the X substituent on the salicylaldehyde portion of each ligand; (2) the degree of ligand delocalization (5-X-SAP^{2-} and 5-X-SSP^{2-} vs 5-X-SAE^{2-} and 5-X-SSE^{2-}); (3) the substitution of a sulfur donor atom in 5-X-SSP^{2-} and 5-X-SSE^{2-} for an oxygen donor atom in 5-X-SAP^{2-} and 5-X-SAE^{2-}, respectively. In general, within a ligand series, as the X substituent becomes more electron withdrawing (X = CH_3O < H < Cl ~ Br < NO_2), the Mo(VI) E_{pc}'s are shifted in the anodic direction. Complexes containing ligands with extended π-delocalization (5-X-SSP^{2-} and 5-X-SAP^{2-}) are easier to reduce than complexes with less extended π-systems (5-X-SSE^{2-} and 5-X-SAE^{2-}). Also, introduction into the ligand of a sulfur atom facilitates reduction (5-X-SSP^{2-} vs 5-X-SAP^{2-} and 5-X-SSE^{2-} vs 5-X-SAE^{2-}).

Similarly, these same ligand features can be considered responsible for influencing the behavior (within and between series) of the ν(Mo=O) frequencies. First however, it is important to understand the details of the molybdenum–oxo oxygen bonding interactions in order to rationalize the experimental data presented here. The molybdenum–oxygen orbital interaction occurring within the *cis*-dioxo-Mo^{2+} structural unit has been described.[16,18,19] As stated by Cotton,[16] the most elementary description of the molybdenum–oxygen bond is that of a double bond. One can identify three components to each of the molybdenum–oxygen bonds, i.e., a σ interaction along the bond axis and two mutually perpendicular π components. In idealized C_{2v} symmetry about the MoO_2 unit, the four O pπ-orbitals transform as a_1, b_1, a_2, and b_2. π-Bonding results from the interaction of the filled O π-orbitals with Mo orbitals of the same symmetry. Though normally depicted as a double bond (Mo=O), six electrons are involved to varying degrees.

(16) Cotton, F. A. *Chem. Uses Molybdenum, Proc. Int. Conf.* **1973**, *1*, 6.
(17) Bachert, J.; Topich, J.; Rheingold, A. Unpublished results.
(18) Stiefel, E. I. *Prog. Inorg. Chem.* **1977**, *22*, 1–223.
(19) Willis, L. J.; Loehr, T. M.; Miller, K. F.; Bruce, A. E.; Stiefel, E. I. *Inorg. Chem.* **1986**, *25*, 4289–4293.

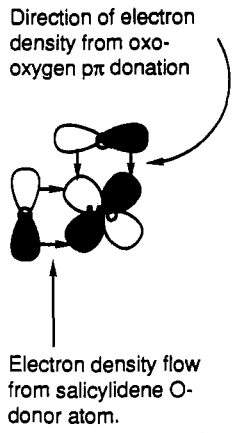

Figure 4. Simplified orbital fragment showing atomic orbital overlap between the salicylidene O donor atom and a molybdenum oxo oxygen.

In dioxo–Mo(VI) species, only the cis stereochemistry is known to exist.[16,19] This is rationalized in terms of maximum utilization of the Mo orbitals of π symmetry. In a *trans*-dioxo configuration, the O pπ orbitals would, as required by symmetry, share the same metal π orbitals.[16,19] Maximum utilization of Mo–O π interactions is accomplished when the oxo ligands adopt a cis configuration. Considering this description of the *cis*-dioxo–Mo unit, the effect of ligand substitution on the ν(Mo=O) can be understood by adopting a model similar to that proposed by Buchler[20] to describe cis and trans effects in transition-metal porphyrins. Buchler uses an intuitive model based on orbital overlap to explain substituent dependent changes in reduction potentials, UV–vis spectra, and metal–oxygen (M=O) stretching vibrations in porphyrin systems. Figure 4 shows a simplified pictorial representation of the interaction between an O pπ orbital (centered on the oxygen donor atom of the salicylidene portion of the ligand), a Mo dπ orbital, and an oxo O pπ orbital. Other orbital interactions of this type are also present (e.g. with the N donor atom). For all ligand systems examined here, there is extensive π-delocalization, inclusive of the fragment depicted in Figure 4. Electron-withdrawing or -donating substituents on the salicylidene ring can induce electron density changes at the molybdenum atom, thereby influencing the Mo=O overlap (these electron density changes also affect the E_{pc} values). Specifically, since the oxo oxygens are pπ donors, greater electron density in the Mo π orbitals (arising from electron-donating substituents) would increase electron repulsions between the Mo π electrons and the oxo O pπ electrons, decreasing the Mo=O overlap, resulting in lower frequency Mo=O stretches. Conversely, when the electron density in the Mo π orbitals is decreased (electron-withdrawing substituents), then repulsions between the oxo O pπ and Mo π electron density are diminished reinforcing Mo=O overlap resulting in increased Mo=O stretching frequencies. The bonding model presented here self-consistently explains the observed trends in both the E_{pc} and ν_{as}(Mo=O).

Figure 5 displays the correlation between ν_{as}(Mo=O) and σ_p for the $Mo^{VI}O_2$(5-X-SAP) series of complexes including $Mo^{VI}O_2$(5,5′-NO_2-SAP) and $Mo^{VI}O_2$(5,4′-NO_2-SAP). Similar correlations between Hammett σ-type parameters and either electrochemical or spectroscopic data have appeared in the literature.[21,22] The data in Figure 5 demonstrate that as the X substituent(s) on the ligands become more electron withdrawing (i.e., in going from OCH_3 to NO_2) the ν_{as}(Mo=O) increases in energy. It is interesting to note the cumulative influence of the two NO_2 substituents in $Mo^{VI}O_2$(5,5′-NO_2-SAP) and $Mo^{VI}O_2$-(5,4′-NO_2-SAP).

In a manner similar to trends observed with E_{pc}, the ν_{as}(Mo=O) values also display trends (for a given set of ligand donor atoms

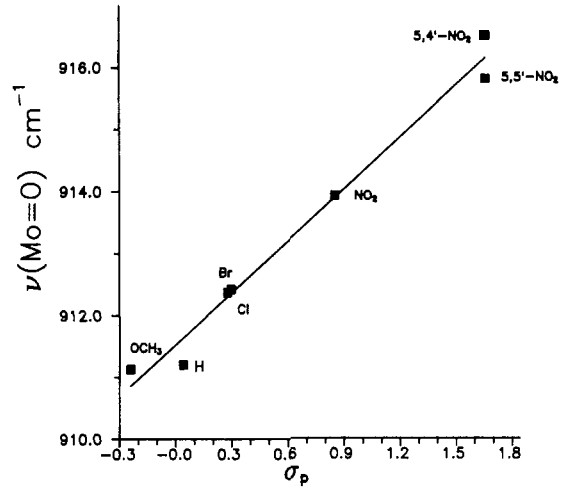

Figure 5. Plot of ν_{as}(Mo=O) vs σ_p for the $Mo^{VI}O_2$(5-X-SAP) series of complexes in DMF. The σ_p value for $Mo^{VI}O_2$(5,4′-NO_2-SAP) and $Mo^{VI}O_2$(5,5′-NO_2-SAP) is 2 times that for the $Mo^{VI}O_2$(5-NO_2-SAP) complex (X = NO_2, Br, Cl, H, CH_3O).

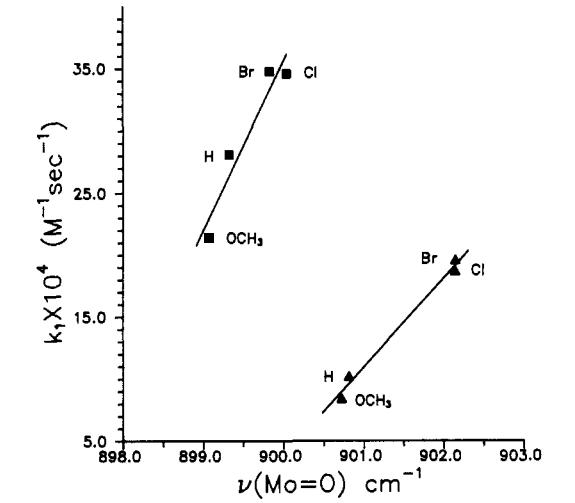

Figure 6. Plot of k_1 vs ν_{as}(Mo=O) for $Mo^{VI}O_2$(5-X-SSE) (■) and $Mo^{VI}O_2$(5-X-SSP) (▲) (X = Br, Cl, H, CH_3O).

ONS vs ONO) depending on the extent of π-electron delocalization within the ligand system. For all members of the 5-X-SAP^{2-} series, the corresponding X-substituted members of the 5-X-SAE^{2-} series display lower values of the ν_{as}(Mo=O) frequency. Similarly, for all members of the 5-X-SSP^{2-} series, the corresponding X-substituted members of the 5-X-SSE^{2-} display lower values of the ν_{as}(Mo=O) frequency, although the mean frequency change between corresponding members is much less for this series than for the $Mo^{VI}O_2$(5-X-SAP) and $Mo^{VI}O_2$(5-X-SAE) series. This observation suggests that as the π-electron delocalization is increased when comparing ligand systems (i.e., 5-X-SSP^{2-} and 5-X-SAP^{2-} vs 5-X-SAE^{2-} and 5-X-SSE^{2-}, respectively), the electron density at the Mo is reduced. This would result in an enhanced Mo π–O pπ interaction, resulting in an increase in ν_{as}(Mo=O) for the more delocalized ligand systems.

Trends in the ν_{as}(Mo=O) frequencies are also observed as a function of the ligand donor atom set (i.e., ONO vs ONS). When a sulfur is substituted for an oxygen atom (5-X-SAP^{2-} vs 5-X-SSP^{2-} and 5-X-SAE^{2-} vs 5-X-SSE^{2-}) one observes a decrease in the ν_{as}(Mo=O) frequencies. Topich[7] explained the variations in the E_{pc} values as a function of O vs S ligand substitution within a given ligand series as being a result of the added covalency imparted by sulfur atom coordination. Enhanced π interactions between metal d-orbitals and empty sulfur d-orbitals decrease the electron density with the *cis*-dioxo–Mo^{2+} unit. This increase in Mo π–S dπ interaction effectively reduces the electron density within the Mo=O bond accounting for the ν_{as}(Mo=O) frequency

(20) Buchler, J. W.; Kokisch, W.; Smith, P. D. *Struct. Bonding (Berlin)* **1978**, *34*, 79–134.
(21) Topich, J. *Inorg. Chim. Acta* **1980**, *46*, L37–L39.
(22) Smith, D. A.; Schultz, F. A. *Inorg. Chem.* **1982**, *21*, 3035–3041.

decrease observed in the $Mo^{VI}O_2$(5-X-SSP) and $Mo^{VI}O_2$(5-X-SSE) complexes vs the corresponding $Mo^{VI}O_2$(5-X-SAP) and $Mo^{VI}O_2$(5-X-SAE) complexes.

Correlations between k_1 and ν_{as}(Mo=O). Figure 6 shows a plot of k_1 (for reaction 1) vs ν_{as}(Mo=O) for the $Mo^{VI}O_2$(5-X-SSP) and $Mo^{VI}O_2$(5-X-SSE) series of complexes. In both cases, as the value of k_1 increases along the series OCH_3 < H < Cl ~ Br, the ν_{as}(Mo=O) increases in the same order. An understanding of the correlation between k_1 and ν_{as}(Mo=O) should be based on how the ν_{as}(Mo=O) trends reflect the availability of the O π^* antibonding orbitals for interaction with the phosphorus lone-pair electrons.

It is necessary to make a distinction between thermodynamic bond dissociation energies (bond strengths, and how vibrational spectra reflect them) and, in this case, how the Mo=O vibrational frequencies reflect in the oxygen atom transfer rate with $PEtPh_2$. The vibrational frequency trends observed here reflect (albeit very small) energy differences between the $v = 0$ and $v = 1$ vibrational levels of the ground-state molecules. However this small energy difference is not (we suggest) what governs the rate of oxygen atom transfer within these complexes. The vibrational frequency changes observed here also reflect the relative energy variations in the bonding and antibonding orbital components of the Mo=O bond.

In general, as a particular chemical bond becomes stronger, the bonding component of the involved molecular orbital becomes more energetically stabilized while the antibonding component concomitantly becomes more destabilized relative to the energetic "center of gravity". Thus, to the extent that vibrational stretching frequencies reflect bond strengths,[16] the data observed here would suggest that along the electron-withdrawing series, OCH_3 < H < Br ~ Cl, the oxo O π^* antibonding component of the Mo=O bond is progressively destabilized in energy. The critical point here is that changes in Mo=O vibrational frequencies reflect changes in the oxo O π^* antibonding orbital energy, and the energy of this orbital apparently has implications on its availability for interaction with the phosphorus lone pair. On the basis of this interpretation, the inherent electronic structure of the $Mo^{VI}O_2$(5-X-SSP) and $Mo^{VI}O_2$(5-X-SSE) complexes apparently modulates the oxo O π^*–phosphorous lone-pair orbital energies in an optimal range for overlap and subsequent reaction, as compared to the $Mo^{VI}O_2$(5-X-SAP) and $Mo^{VI}O_2$(5-X-SAE) complexes, which display negligible reactivity toward $PEtPh_2$. Hence, the observed correlation between k_1 and ν_{as}(Mo=O).

Some comment is necessary regarding the comparison of the $Mo^{VI}O_2$(5-X-SSP) and $Mo^{VI}O_2$(5-X-SSE) reactivities with that of $Mo^{VI}O_2(S_2CNEt_2)_2$. With the $Mo^{VI}O_2$(5-X-SSP) and $Mo^{VI}O_2$(5-X-SSE) series, as the ν(Mo=O) increases so does the specific rate constant (k_1) along the series $Mo^{VI}O_2$(5-X-SSE) < $Mo^{VI}O_2$(5-X-SSP), and OCH_3 < H < Cl ~ Br. On the basis of this behavior one might expect that the $Mo^{VI}O_2(S_2CNEt_2)_2$ system, with a lower ν(Mo=O), would have a lower specific rate constant. In fact the rate constant for this system is larger than that for the $Mo^{VI}O_2$(5-X-SSE) and $Mo^{VI}O_2$(5-X-SSP) series. This would indicate that the trends observed for the $Mo^{VI}O_2$(5-X-SSE) and $Mo^{VI}O_2$(5-X-SSP) series are not necessarily generalizable to other ligand systems, thus one should restrict comparisons to structural analogues. However, since the oxygen atom transfer mechanism is presumably the same for both $Mo^{VI}O_2$(5-X-SSE) and $Mo^{VI}O_2$(5-X-SSP) and $Mo^{VI}O_2(S_2CNEt_2)_2$, a study undertaken for the $Mo^{VI}O_2(S_2CNR_2)_2$ series involving systematic electronic variations may reveal similar correlations between ν(Mo=O) and the specific rate constant for oxygen atom transfer. Thus, for analogous systematically varied ligand systems where the oxygen atom transfer mechanism is the same as that described here, ν(Mo=O) should provide information for the design of complexes which exhibit a higher reactivity toward organophosphines, and possibly other biologically relevant substrates.

Conclusions

We have shown that for the $Mo^{VI}O_2$(5-X-SSP), $Mo^{VI}O_2$(5-X-SSE), $Mo^{VI}O_2$(5-X-SAP), and $Mo^{VI}O_2$(5-X-SAE) complexes, the ν_{as}(Mo=O) stretching frequencies vary as a function of (1) the X substituent on the tridentate Schiff base ligand, (2) the extent of π-electron delocalization within the ligand framework, and (3) the ligand donor atom set (ONS vs ONO). Also, we have shown the correlation between ν_{as}(Mo=O) and k_1 for the oxygen atom transfer reaction for $Mo^{VI}O_2$(5-X-SSP) and $Mo^{VI}O_2$(5-X-SSE) complexes with $PEtPh_2$. The ν_{as}(Mo=O) reflects changes in the oxo O π^* antibonding orbital energy within a substituted series of complexes. The energy difference between the oxo O π^* and the phosphorus lone-pair orbitals governs the tendency for these orbitals to interact, contributes to the activation energy for this reaction, and hence affects the rate of oxygen atom transfer.

Registry No. 5,5′-NO_2-SAP-H_2, 138061-29-7; 5,4′-NO_2-SAP-H_2, 112383-44-5; *cis*-MoO_2(5-Br-SSP)·DMF, 89352-58-9; *cis*-MoO_2(5-Cl-SSP)·DMF, 89352-57-8; *cis*-MoO_2(5-H-SSP)·DMF, 89396-11-2; *cis*-MoO_2(5-OCH_3-SSP)·DMF, 89352-56-7; *cis*-MoO_2(5-Br-SSE)·DMF, 138061-30-0; *cis*-MoO_2(5-Cl-SSE)·DMF, 138061-31-1; *cis*-MoO_2(5-H-SSE)·DMF, 138061-32-2; *cis*-MoO_2(5-OCH_3-SSE)·DMF, 138061-33-3; *cis*-MoO_2(5,5′-NO_2-SAP), 138061-34-4; *cis*-MoO_2(5,4′-NO_2-SAP)·DMF, 138061-35-5; *cis*-MoO_2(5-NO_2-SAP)·DMF, 138061-36-6; *cis*-MoO_2(5-Br-SAP)·DMF, 138061-37-7; *cis*-MoO_2(5-Cl-SAP)·DMF, 138061-38-8; *cis*-MoO_2(5-H-SAP)·DMF, 75908-27-9; *cis*-MoO_2(5-OCH_3-SAP)·DMF, 138061-39-9; *cis*-MoO_2(5-NO_2-SAE)·DMF, 138061-40-2; *cis*-MoO_2(5-Br-SAE)·DMF, 138061-41-3; *cis*-MoO_2(5-Cl-SAE)·DMF, 138061-42-4; *cis*-MoO_2(5-H-SAE)·DMF, 138061-43-5; *cis*-MoO_2(5-OCH_3-SAE)·DMF, 138089-53-9; *cis*-$MoO_2(S_2CNEt_2)_2$, 18078-69-8; $MoO_2(acac)_2$, 17524-05-9; $PEtPh_2$, 607-01-2; 5-nitrosalicylaldehyde, 97-51-8; 2-amino-5-nitrophenol, 121-88-0; 2-amino-4-nitrophenol, 99-57-0.